



## FAST RESPONSE UV PHOTODETECTOR BASED ON ALIGNED ARRAYS OF ANATASE TiO<sub>2</sub> NANOTUBES

Khaled M. N. CHAHROUR<sup>1\*</sup>


<sup>1</sup>Karabük University, Faculty of Engineering, Department of Mechanical Engineering, 78050, Karabük, Türkiye

**Abstract:** Aligned arrays of anatase TiO<sub>2</sub> nanotubes on a Ti sheet were created by a dual-step electrochemical anodizing treatment and extended calcination step at 400 °C under an ambient atmosphere, as shown in FESEM images. A diffuse reflectance approach was adopted to measure the energy bandgap is 3.42 eV. The nanotubular pattern is utilized to assemble a fast-response UV photodetector as recognized by Metal-Semiconductor-Metal assembly. The photodetector exhibited excellent UV sensitivity, attributed to the anatase phase of the TiO<sub>2</sub> nanotube arrays. The photodetection testing confirmed adept detection of UV photon illumination with excellent stability and repeatability. The UV photodetection performance exhibited a current gain value of 6, a response time (T<sub>on</sub>) of 0.98, 0.97, and 0.92 seconds, and a recovery time (T<sub>off</sub>) of 0.97, 0.95, and 0.94 seconds at a biased potential of 3, 4, and 5 V, respectively. The findings of this research corroborate the promising nature of the UV photodetector fabricated utilizing anatase nanotube arrays, exhibiting its immense potential for applications in the UV spectrum.

**Keywords:** Anatase-1, Anodizing treatment-2, TiO<sub>2</sub> nanotubes-3, UV photodetector-4

\*Corresponding author: Karabük University, Faculty of Engineering, Department of Mechanical Engineering, 78050, Karabük, Türkiye

E mail: khaledchahrou@karabuk.edu.tr (K. M. N. CHAHROUR)

Khaled M. N. CHAHROUR  <https://orcid.org/0000-0002-8799-3468>

Received: April 17, 2024

Accepted: July 06, 2024

Published: July 15, 2024

Cite as: Chahrou KMN. 2024. Fast response UV photodetector based on aligned arrays of anatase TiO<sub>2</sub> nanotubes. BSJ Eng Sci, 7(4): 736-742.

### 1. Introduction

Various features of nanomaterials have garnered significant attention in nano-optoelectronic devices due to their unique electronic properties (Khudiar et al., 2022; Ibrahim et al., 2023). Aligned arrays of anatase TiO<sub>2</sub> nanotube arrays (ATNT) synthesized by electrochemical anodizing treatment of Ti sheet and followed by calcination at high temperatures which has been frequently scrutinized over the past decade, exhibition prominent potential uses in nano-optoelectronics devices (Chahrou, et al., 2019; Ikreedeeh et al., 2024). As compared to crystalline thin film and randomly oriented nanostructures, the ATNT features are assumed to maintain unidirectional charge carriers inside the nanotubes that thrust further charge carriers driven which is crucial for the nano-optoelectronics device's performance. Numerous recent studies have highlighted that the transport speed of charge carriers within nanotubes is slower compared to other nanostructured films attributed to the presence of exciton-like traps that hinder the charge carriers' mobility and cause reducing of the efficiency of ATNT-based nano-optoelectronics devices (Richter and Schmuttenmaer, 2010).

The exciton-like traps in ATNT architecture could be lowered by calcination at high temperatures in an oxygen environment, which pushes for a decrease in oxygen

vacancies. In addition, the ATNT architecture's main impact is the photo-activity, which is only sustained around 400°C. Subsequently, this temperature value represents a transformation from amorphous to anatase phase and the fulfilment of orientation and arrangement might be preserved. Maintaining the nanotubular configuration at a temperature of 400°C with decreased exciton-like traps continues to be a challenge for attaining competent photoactivity of the TiO<sub>2</sub> nanotubular based nano-optoelectronic designs (Rao and Roy, 2014). Moreover, the large surface area, well-defined charge carrier transport channels, and selective UV absorption properties of ATNT architecture effectively enable UV band detection (Zhang et al., 2016). Numerous TiO<sub>2</sub> nanostructures dependent on UV photodetection experiments have been described (Zou et al., 2010; Zheng et al., 2017; Chahrou et al., 2020a; Li et al., 2022). Few experiments have been performed to exploit UV photodetection devices built on the anatase TiO<sub>2</sub> nanotube arrays matching to metal-semiconductor-metal. Anatase TiO<sub>2</sub> nanotube arrays, with their distinctive morphological characteristics, could potentially be considered an optimal substitute for ultraviolet photodetection (Yu et al., 2018).

In this study, a simple calcination method was employed in Laboratory atmosphere conditions to fabricate a mono-phase anatase TiO<sub>2</sub> nanotube array on a Ti



substrate, enabling the creation of a UV photodetector. The UV photocurrent properties were meticulously examined and demonstrated that the photodetector exhibited excellent gain, rapid response, consistent repeatability, and substantial stability in photodetection over the UV band.

## 2. Materials and Methods

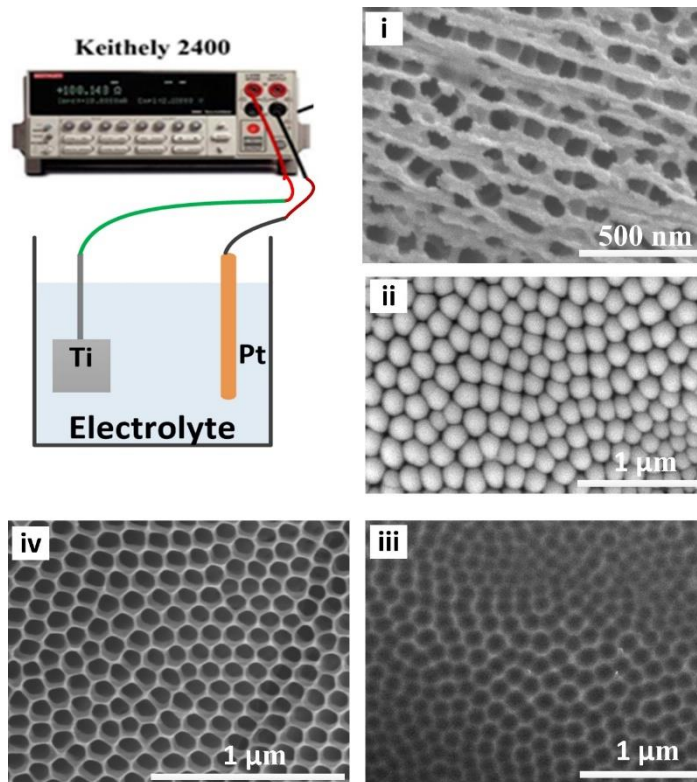
A dual-step electrochemical anodizing treatment has been experimented with convenient controllable parameters in the ethanol glycol to grow aligned arrays of anodic TiO<sub>2</sub> nanotubes film. This electrochemical anodizing treatment was depicted in detail in earlier published research (Chahrour et al., 2019; Chahrour et al., 2020b; Chahrour et al., 2020c). Amorphous TiO<sub>2</sub> nanotubes film was calcined at 400°C under ambient conditions in a tube furnace for 3 hours to transform them into anatase TiO<sub>2</sub> nanotube arrays. The single-phase anatase nanotube arrays were amenable for constructing a metal-semiconductor-metal UV photodetector. Nickel element was chosen as the Schottky metal contacts with a thickness of 200 nm were deposited over anatase TiO<sub>2</sub> nanotube arrays film via radio frequency (RF) sputtering (Edwards A500, UK) at a base pressure of  $1.5 \times 10^{-5}$  mbar at room temperature onto a metallic mask, following the design of two-terminal electrodes with four fingers on each terminal. The current-voltage (I-V) distinctive characteristic and

photo-current response time for the assembled apparatus were assessed at altered bias potentials (3, 4, and 5 V) and under UV photon illumination (365 nm, 1.5 mW/cm<sup>2</sup>) by applying Keithley source meter (model No. 2400) at research laboratory atmosphere.

The ATNT films were shown by FESEM (Nova NanoSem model-450). Crystalline structures were realized through High-Resolution XRD (PANalytical X'pert PRO MRD PW3040) with a CuK- $\alpha$  source of 0.154 nm wavelength. Diffuse reflectance spectrum was acquired from 200 to 800 nm via applying a UV-VIS-NIR spectrophotometer (Agilent Cary model-5000).

## 3. Results and Discussion

Figure 1 exhibitions FESEM overview images for summarizing the microstructural procedure of manufactured nanoporous TiO<sub>2</sub> nanotubes: (i) irregular nanoporous TiO<sub>2</sub> nanotubes film manufacture during the first-step anodizing process on the Ti sheet, (ii) the well-organized bottom view of the irregular nanoporous TiO<sub>2</sub> film, (iii) formation of a regular domain of indentations on Ti sheet after denudation of nanoporous TiO<sub>2</sub> film, and (iv) highly-organized hexagonal nanoporous TiO<sub>2</sub> nanotubes film after the second-step of anodizing treatment. The nanopores have grown promisingly on the indentations of the Ti sheet, which caused the creation of admirable ordered hexagonal nanoporous structures of amorphous TiO<sub>2</sub> nanotubes film.



**Figure 1.** presents FE-SEM overview images for summarizing the microstructural procedure of manufactured admirable ordered hexagonal nanoporous anodic TiO<sub>2</sub> nanotubes. (i) irregular nanoporous TiO<sub>2</sub> nanotubes film during the first-step anodization, (ii) the well-organized bottom view of the irregular nanoporous TiO<sub>2</sub> film, (iii) formation of a regular domain of indentations on Ti sheet after denudation of nanoporous TiO<sub>2</sub> film, and (iv) highly-organized hexagonal nanoporous TiO<sub>2</sub> nanotubes film after the second-step of anodization.

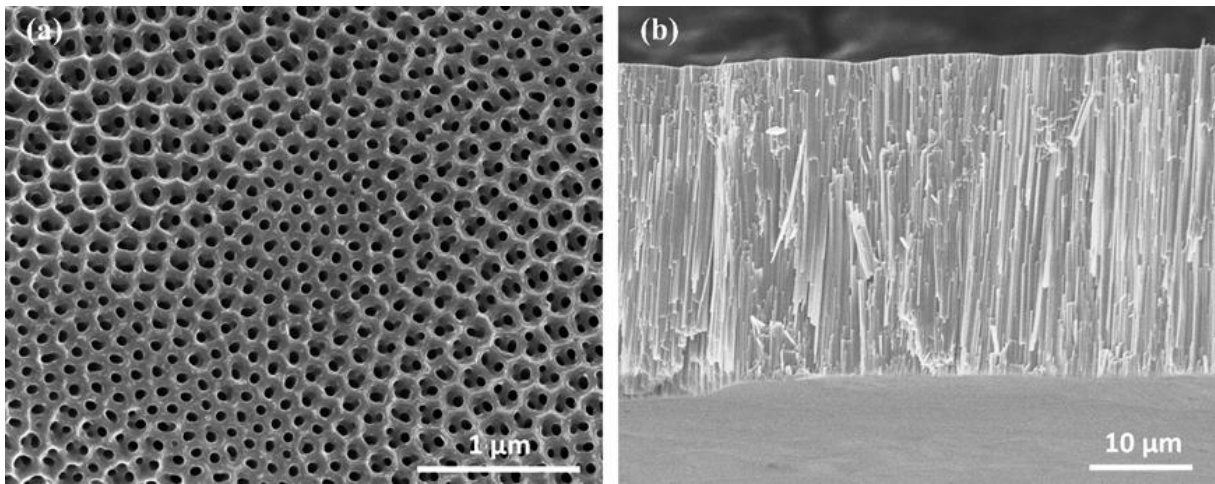


**Figure 2.** (a) FESEM prototypes expose the overhead view and (b) the lateral view of calcined anodic TiO<sub>2</sub> nanotube arrays film at 400°C, respectively.

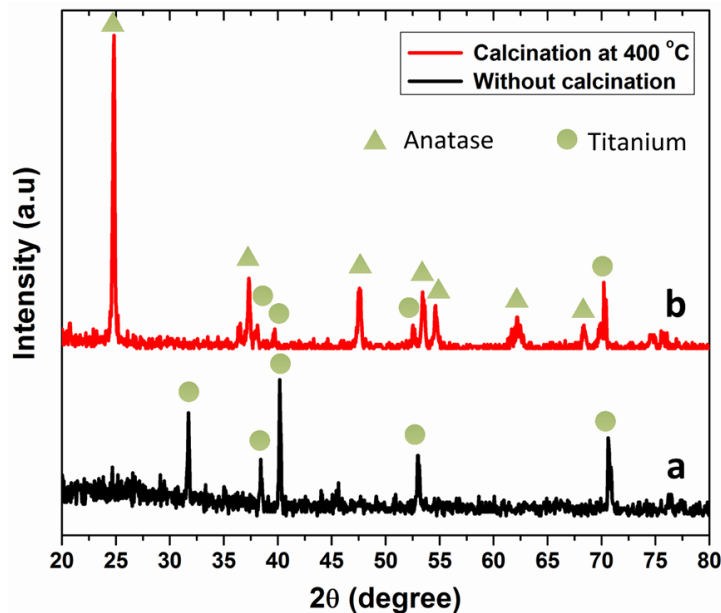


**Figure 3.** XRD distribution of anodic TiO<sub>2</sub> nanotube arrays film (a) without calcination (b) with calcination at 400°C.

Figure 2(a) depicts an overhead FESEM image view of the ATNT film extended calcination process at 400°C, revealing a hexagonal highly structured honeycomb-like web assembly with an average pore diameter exceeding 90 nm. Figure 2 (b) denotes the FESEM image lateral view for the ATNT film, where the tubular walls appear to be planner and flat. It is quite apparent that the tubular morphology of the calcined sample has significant characteristics. When the nanotubes were focused on, the swelled edges of honeycomb-web designed nanotubes can be observed, and the tubular assemblies were sustained at such a high-temperature calcination process.

Figure 3(a) presents the x-ray diffraction distribution of the amorphous ATNT film without calcination as a pristine sample, where no peaks of the anatase phase were observed only exhibiting five distinct peaks that can be attributed to the underlying Titanium substrate: (100), (002), (101), (102), and (103) at 31.62°, 38.37°,

40.18°, 52.93°, and 70.6°, respectively. Figure 3 (b) presents the x-ray diffraction distribution for ATNT film calcined at 400°C. Correspondingly, four record standard peaks can be credited to Titanium as well: (002), (101), (102), and (103) at 38.37°, 40.18°, 52.93°, and 70.6°, respectively. The anatase standard peaks showed at 25.1°, 37.5°, 47.6°, 53.8°, 55°, 62.21° and 68.6° were distinctly knowing over the crystalline patterns (101), (112), (200), (105), (211), (204) and (116). However, some peaks due to the anatase phase partly coincided with the crystalline phase of Titanium (Chahrour et al., 2023).

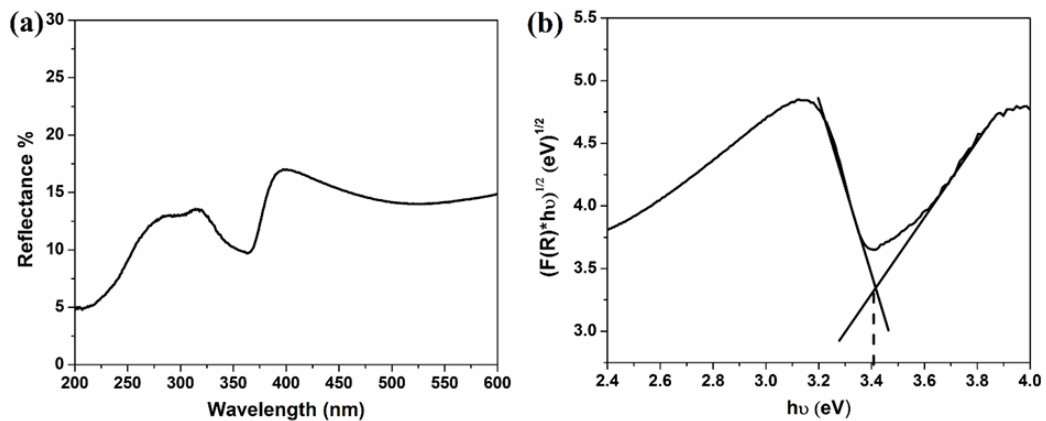
A diffuse reflectance approach was adopted to measure the energy bandgap of the TiO<sub>2</sub> nanotubes. The experiment was accomplished in a wide spectral range from 200 nm to 800 nm, as depicted in Figure 4 (a). The Kubelka-Munk relationship  $F(R)$  was implemented to compute the energy bandgap, which is represented by Equation (1) (Aper et al., 2021).

$$F(R) = \frac{(1 - R)^2}{2R} \quad (1)$$

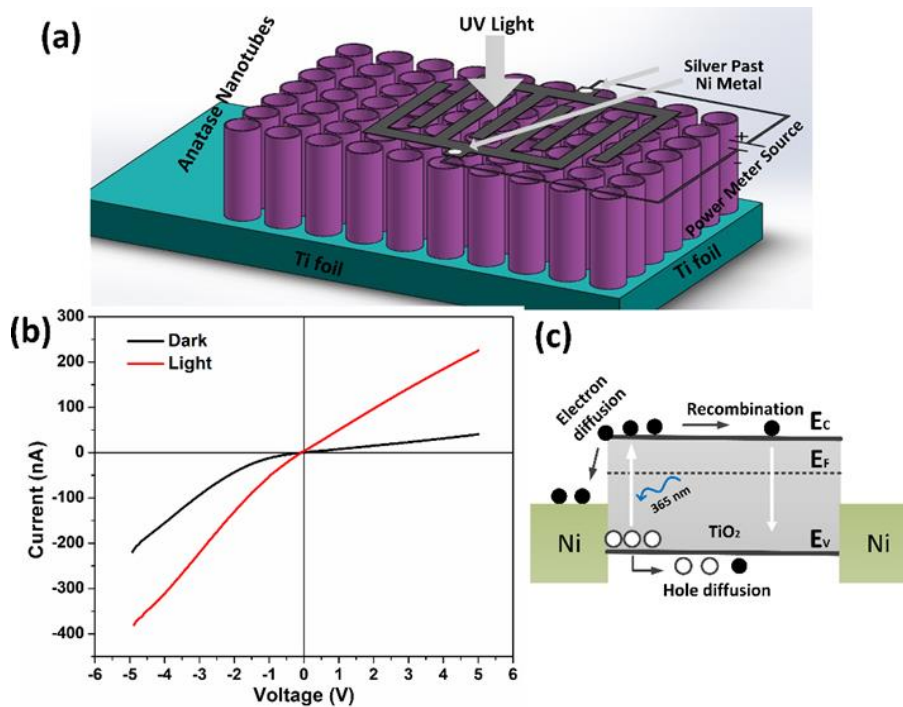
Figure 4 (b) exhibits  $(F(R) hv)^{1/2}$  as a function of the bandgap ( $hv$ ) plot. The indirect energy band gap ( $E_g$ ) of anatase  $TiO_2$  nanotube arrays could be computed by assuming a direct portion of the  $(F(R)hv)^{1/2}$  to pass across the bandgap ( $hv$ ) axis. The bandgap was estimated at 3.42 eV for AATNTs film. This quantity is comparable with the earlier studies (Jubu et al., 2022; Jubu et al., 2023). Additionally, this established value of the energy bandgap enables significant UV light absorption to generate excited pairs of electron-hole combinations.

Figure 5(a) presents a diagram of the apparatus employed to assess the current-voltage ( $I-V$ ) behaviors and photo-response in both dark and UV irradiation. Figure 5(b) demonstrates the distinctive current-voltage ( $I-V$ ) behaviors observed when the apparatus is

darkened and illuminated with 365 nm light at 1.5  $mW/cm^2$ , characterized by a proportional relationship and nonlinear curve behavior. This direct observation strongly substantiates the formation of a Schottky potential barrier between the Ni metal probes and the  $TiO_2$  nanotubes. Moreover, the Fermi energy of Ni metal contacts becomes lower than the Fermi energy in the  $TiO_2$  nanotubes, which reduces the potential barrier region across it (Gong et al., 2017; Rosli et al., 2020). The photocurrent process mainly involves generating electron-hole pairs using focused UV radiation with a wavelength of 365 nm, then brought together in the Schottky barrier region between  $TiO_2$  nanotubes and Ni metal contacts, where applied bias potential triggers the separation of electron-hole pairs, in which photoelectrons are diffused in the Ni metal probes (Abdalrheem et al., 2019) as illustrated in Figure 5 (c).



**Figure 4.** (a) Diffuse reflectance spectrum and (b) Tauc plot of the  $(F(R) hv)^{1/2}$  vs  $hv$  of anodic anatase  $TiO_2$  nanotube arrays film calcined at  $400^\circ C$ .



**Figure 5.** (a) Diagram of the UV photodetector apparatus. (b) The current-voltage ( $I-V$ ) behaviors of the photodetector apparatus in both dark and light UV luminescence. (c) Schematic-diagram for the creation process of electron-hole pairs for Ni- $TiO_2$  nanotubes-Ni photodetector under UV luminescence.

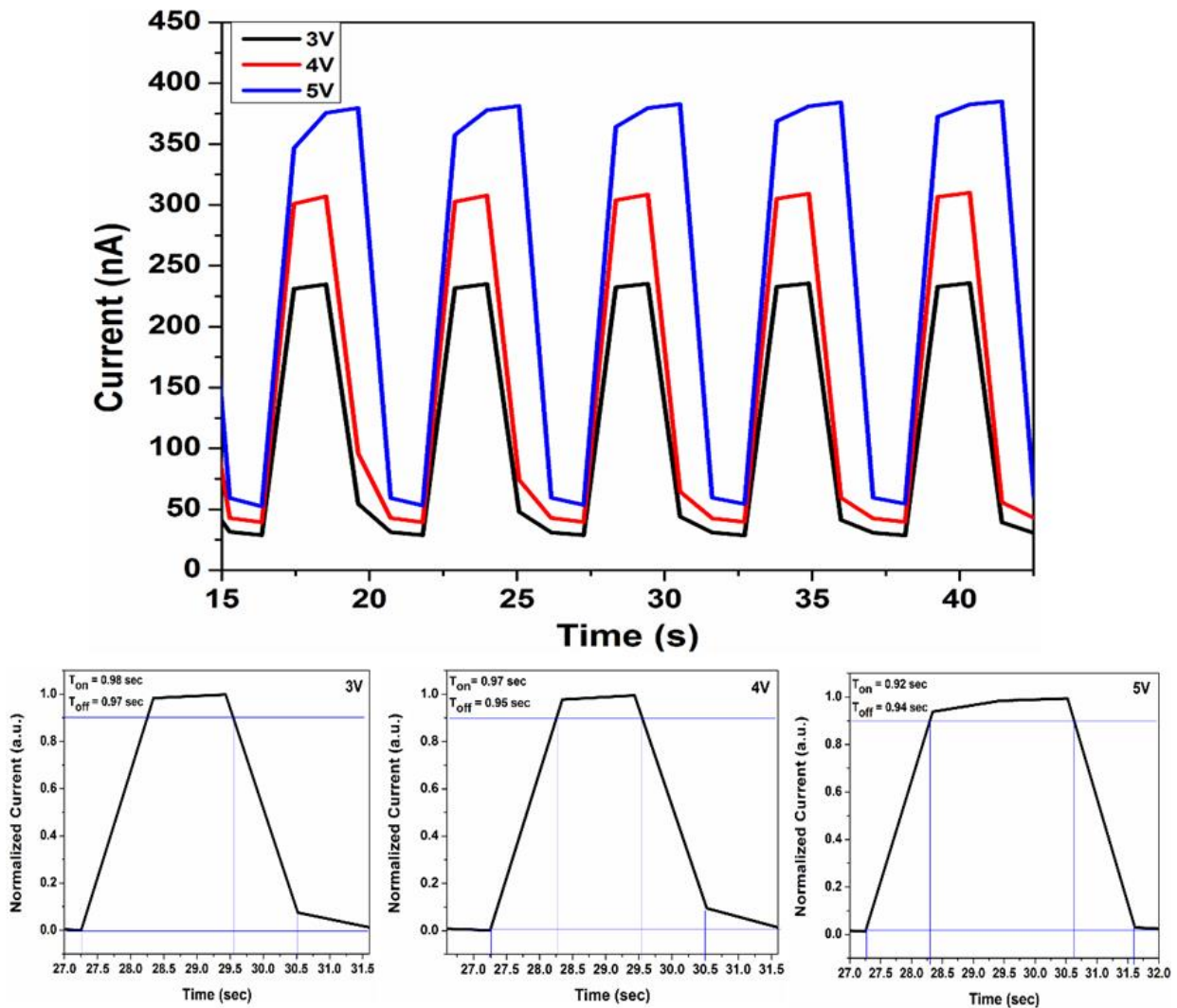


**Figure 6.** Photo-response curves of the photodetector apparatus at bias potentials 3, 4, and 5 V, respectively. Normalized current-time behaviors indicate the response and recovery times at 3, 4, and 5 V, respectively.

Photocurrent gain ( $g$ ) is a valuable factor that is employed to evaluate the photodetector performance, which can be formulated by Equation (2) (AlShammari et al., 2021).

$$g = \frac{I_{light}}{I_{dark}} \quad (2)$$

$I_{light}$  is the light current,  $I_{dark}$  is the dark current. The quantitative gain of the photodetector apparatus amounted from Figure 5 (b) to nearly 6 at the bias potential of 5 V. The remarkable increase in photocurrent generation appears from the enhanced surface per volume ratio and superior crystalline nature of TiO<sub>2</sub> nanotubes. The larger surface area of the nanotube arrays accommodates more UV photon absorption, effectively accumulating more light energy and boosting the photocurrent output. Additionally, the exceptional crystalline structure of the nanotubes minimizes the formation of trapping sites or vacancies that can impair charge carriers, significantly enhancing the photo-response and overall efficiency of the system (Chahrour et al., 2016).

Figure 6 displays the current-time curves obtained at 3,

4, and 5 V bias potentials when the UV photon illumination of 365 nm was turned on and off repeatedly. The peak current remains consistent for multiple cycles across all applied bias potentials, highlighting the exceptional repeatability and stability of the device. Additionally, the near-instantaneous rise and fall responses with minimum exponential in the photocurrent pulses signify that the photocurrent originates from direct inter-band electron transitions. Moreover, the increase in photocurrent with increasing bias potential indicates an enhancement in charge carrier drift velocity due to a short in charge carrier diffusion time. To assess the UV photodetector's performance, key parameters such as the response time ( $T_{on}$ ) is defined as the duration it takes for the current to rise to 90% of its saturation value, and recovery time ( $T_{off}$ ) is defined as the duration for current to drop from 90% of its saturation value were measured. As depicted in Figure 6, by extending the time duration for switching on and off the UV light source, it was observed that  $T_{on}$  values are 0.98, 0.97, and 0.92 seconds, respectively, and  $T_{off}$  values are 0.97, 0.95, and 0.94 seconds at bias potentials of 3, 4, and 5 V, respectively. This points out that the  $T_{on}$  and  $T_{off}$

recorded in this research are moderately faster compared to previously reported (Wang et al., 2015; Ng et al., 2018).

#### 4. Conclusion

In the final remarks, well-aligned arrays of TiO<sub>2</sub> nanotubes were produced on Ti sheets using a dual-step electrochemical anodization process, followed by calcination at 400°C under ambient conditions. The remarkable morphological properties of these aligned arrays of anatase nanotubes were utilized to create UV photodetector devices exhibiting superior photoresponse characteristics, remarkable repeatability, and exceptional stability over time. The outstanding implementation of these devices confirms that TiO<sub>2</sub> nanotube arrays with anatase phase uniformity hold strong potential in the domain of nano-optoelectronic devices.

#### Author Contributions

The percentage of the author contributions is presented below. The author reviewed and approved the final version of the manuscript.

	K.M.N.C.
C	100
D	100
S	100
DCP	100
DAI	100
L	100
W	100
CR	100
SR	100
PM	100
FA	100

C=Concept, D= design, S= supervision, DCP= data collection and/or processing, DAI= data analysis and/or interpretation, L= literature search, W= writing, CR= critical review, SR= submission and revision, PM= project management, FA= funding acquisition.

#### Conflict of Interest

The author declared that there is no conflict of interest.

#### Ethical Consideration

Ethics committee approval was not required for this study because of there was no study on animals or humans.

#### Acknowledgements

The corresponding author gratefully acknowledges the financial support provided by the Scientific Research Projects Coordination Unit of Karabuk University under grant no. KBUBAP-22-ABP-151.

#### References

AbdAlrheem R, Yam F, Ibrahim AR, Lim H, Beh K, Ahmed AA, Oglat AA, Chahrour KM, Farhat OF, Afzal N. 2019. Improvement in photodetection characteristics of

graphene/p-Silicon heterojunction photodetector by PMMA/graphene cladding layer. *J Electronic Mater*, 48: 4064-4072.

AlShammari A, Halim M, Yam F, Chahrour K, Raypah M, Kaus N. 2021. The effect of spray cycles on the morphological, structural, and optical properties of rGO thin film deposited using spray pyrolysis technique. *Mater Sci Semiconductor Proces*, 127: 105655.

Aper T, Yam F, Saw K, Beh KP, Chahrour KM. 2021. Atmospheric pressure chemical vapor deposition of indium oxide nanostructured films for photoelectrochemical application. *Results Physics*, 24: 104187.

Chahrour KM, Ahmed NM, Hashim M, Elfadill NG, Bououdina M. 2016. Self-assembly of aligned CuO nanorod arrays using nanoporous anodic alumina template by electrodeposition on Si substrate for IR photodetectors. *Sensors Actuators A: Physical*, 239: 209-219.

Chahrour KM, Ooi PC, Nazeer AA, Al-Hajji LA, Jubu PR, Dee CF, Ahmadipour M, Hamzah AA. 2023. CuO/Cu/rGO nanocomposite anodic titania nanotubes for boosted non-enzymatic glucose biosensors. *New J Chem*, 47(16): 7890-7902.

Chahrour KM, Yam F, Abdalrheem R. 2019. High-performance UV photodetector of anodic rutile TiO<sub>2</sub> nanotube arrays. *Mater Lett*, 248: 161-164.

Chahrour KM, Yam F, Eid A, Nazeer AA. 2020b. Enhanced photoelectrochemical properties of hierarchical black TiO<sub>2</sub>-x nanolaces for Cr (VI) photocatalytic reduction. *Int J Hydrogen Energy*, 45(43): 22674-22690.

Chahrour KM, Yam F, Eid A. 2020a. Water-splitting properties of bi-phased TiO<sub>2</sub> nanotube arrays subjected to high-temperature annealing. *Ceramics Int*, 46(13): 21471-21481.

Chahrour KM, Yam F, Lim H, Abdalrheem R. 2020c. Synthesis of anodic TiO<sub>2</sub> nanotube arrays annealed at 700° C for UV photodetector. *J Physics: Conf Ser*, 1535: 012012.

Chahrour KM, Yam F, Samuel JJ, Abdalrheem R, Beh K, Lim H. 2019. Controlled synthesis of vertically aligned honeycomb TiO<sub>2</sub> nanotube arrays: effect of high-temperature annealing on physical properties. *Appl Physics A*, 125: 1-9.

Gong XX, Fei GT, Fu WB, Zhong BN, Gao XD, De Zhang L. 2017. Metal-semiconductor-metal infrared photodetector based on PbTe nanowires with fast response and recovery time. *Appl Surface Sci*, 404: 7-11.

Ibrahim MA, Verrelli E, Lai KT, Cheng F, O'Neill M. 2023. Effect of atmospheric conditions on ultraviolet photoconductivity of zinc oxide nanoparticles. *J Appl Sci Nanotechnol*, 3(1): 115-123.

Ikreedeegh RR, Hossen MA, Tahir M, Abd Aziz A. 2024. A comprehensive review on anodic TiO<sub>2</sub> nanotube arrays (TNTAs) and their composite photocatalysts for environmental and energy applications: Fundamentals, recent advances and applications. *Coord Chem Rev*, 499: 215495.

Jubu PR, Chahrour KM, Muhammad A, Landi S, Obaseki O, Igbawua T, Gundu A, Chahul H, Yam F. 2023. Considerations about the determination of optical bandgap from diffuse reflectance spectroscopy using the Tauc plot. *J Optics*. 2024: 1-11.

Jubu PR, Chahrour KM, Yam F, Awoji O, Yusof Y, Choo EB. 2022. Titanium oxide nanotube film decorated with β-Ga<sub>2</sub>O<sub>3</sub> nanoparticles for enhanced water splitting properties. *Solar Energy*, 235: 152-162.

Khudiar SS, Nayef UM, Mutlak FA. 2022. Preparation and characterization of porous silicon for photodetector applications. *J Appl Sci Nanotechnol*, 2(2): 64-69.

- Li Z, Li Z, Zuo C, Fang X. 2022. Application of nanostructured TiO<sub>2</sub> in UV photodetectors: A review. *Adv Mater*, 34(28): 2109083.
- Ng S, Yam FK, Sohimee SN, Beh KP, Tneh SS, Cheong YL, Hassan Z. 2018. Photoelectrochemical ultraviolet photodetector by anodic titanium dioxide nanotube layers. *Sensors Actuators A: Physical*, 279: 263-271.
- Rao BM, Roy SC. 2014. Anatase TiO<sub>2</sub> nanotube arrays with high temperature stability. *RSC Adv*, 4(72): 38133-38139.
- Richter C, Schmuttenmaer CA. 2010. Exciton-like trap states limit electron mobility in TiO<sub>2</sub> nanotubes. *Nature Nanotechnol*, 5(11): 769-772.
- Rosli N, Halim MM, Chahrour KM, Hashim MR. 2020. Incorporation of zinc oxide on macroporous silicon enhanced the sensitivity of macroporous silicon MSM photodetector. *ECS J Solid State Sci Technol*, 9(10): 105005.
- Wang L, Yang W, Chong H, Wang L, Gao F, Tian L, Yang Z. 2015. Efficient ultraviolet photodetectors based on TiO<sub>2</sub> nanotube arrays with tailored structures. *RSC Adv*, 5(65): 52388-52394.
- Yu A, Zhan S, Qiu L, Wang X, Yang H, Li Y. 2018. Ultraviolet detector with ultrahigh responsivity based on Anatase TiO<sub>2</sub> nanotubes array modified with (001) exposed nanofacets. *Vacuum*, 151: 237-242.
- Zhang DY, Ge CW, Wang JZ, Zhang TF, Wu YC, Liang FX. 2016. Single-layer graphene-TiO<sub>2</sub> nanotubes array heterojunction for ultraviolet photodetector application. *Appl Surface Sci*, 387: 1162-1168.
- Zheng L, Hu K, Teng F, Fang X. 2017. Novel UV-visible photodetector in photovoltaic mode with fast response and ultrahigh photosensitivity employing Se/TiO<sub>2</sub> nanotubes heterojunction. *Small*, 13(5): 1602448.
- Zou J, Zhang Q, Huang K, Marzari N. 2010. Ultraviolet photodetectors based on anodic TiO<sub>2</sub> nanotube arrays. *J Physical Chem C*, 114(24): 10725-10729.